Molecular Recipe for -Secretase Modulation from Computational Analysis of 60 Active Compounds

Tang, Ning; Somavarapu, Arun Kumar; Kepp, Kasper Planeta

Published in:
ACS Omega

Link to article, DOI:
10.1021/acsomega.8b02196

Publication date:
2018

Document Version
Publisher's PDF, also known as Version of record

ACS OMEGA

Article

Cite This: ACS Omega 2018, 3, 18078−18088

http://pubs.acs.org/journal/acsodf

Molecular Recipe for γ-Secretase Modulation from Computational Analysis of 60 Active Compounds

Ning Tang, Arun K. Somavarapu, and Kasper P. Kepp*

Department of Chemistry, Technical University of Denmark, Kemitorvet 206, DK-2800 Kongens Lyngby, Denmark

Supporting Information

ABSTRACT: γ-secretase is a membrane protease complex that catalyzes the cleavage of the amyloid precursor protein to produce the infamous Aβ peptides involved in Alzheimer's disease (AD). Major efforts aim to modulate this cleavage to reduce the formation of longer, more toxic Aβ peptides, yet the molecular basis of this modulation remains unknown. We studied the quantitative structure−activity relations using a carefully curated data set of 60 experimental EC_{50} values (the GSL60 data set). To ensure adequate optimization, we used 10 different methods to build the models, Y-randomization, 10-fold repeated cross-validation, and explicit external validation on a secondary data set. Neural network optimization best reproduced experimental log EC_{50}. We find that only four descriptors, the number of hydrogen-bond acceptor sites, the topology of the drug, the dehydration energy, and the binding energy to γ-secretase, define most of the potency of γ-secretase modulators. We explain this as a compromise between the binding free energy to the protein and required hydrogen bond networks in the actual modulatory sites. Our model suggests that many molecules can modulate cleavage simply by contributing their binding energy to stabilize the compact ternary complex with C99. This result is in line with a mechanism, referred to here as FIST (Fit, Stay, Trim), where stronger binding to the semiopen state leads to longer retention time and maximal C99 trimming to produce shorter innocent Aβ peptides, whereas AD-causing PSEN1 mutations favor the open state by reducing hydrophobic packing, retention time, and trimming and modulators strengthen interactions in the ternary complex to increase the C99 retention time and trimming, ultimately producing more short, nonpathogenic Aβ peptides. Our results may aid the development of new γ-secretase modulators with optimal hydrogen bonds, shape, and hydrophobicity but more importantly provide a structural−chemical model of the modulation of Aβ production.

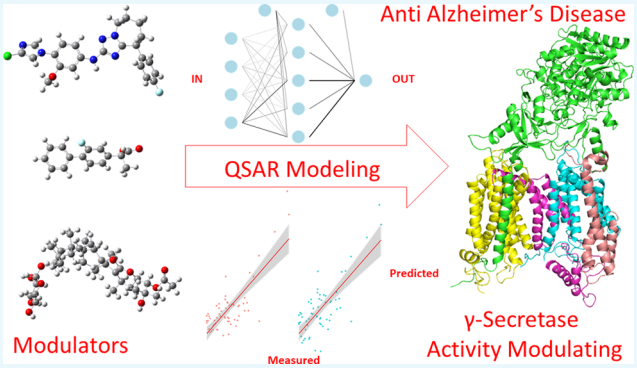

INTRODUCTION

Alzheimer's disease (AD) is a devastating chronic neurodegenerative disease, characterized by progressive loss of memory, cognitive impairment, and personality change; it constitutes up to 60% of all dementia cases and thus affects more than 30 million people worldwide.[1,2] Despite many years of research and attempts to develop therapies, there is still no cure for AD or even an effective therapy to significantly stall AD symptoms for more than a few months.[3] This is largely because the disease is biochemically extremely complex and accordingly mainly occurs sporadically, with many risk modifiers. Thus, there is an urgent need to develop new molecular insight and strategies for prevention and treatment.

Accumulation of senile plaques composed of aggregates of longer forms of β-amyloid peptides ($Aβ_{42}$ or $Aβ_{43}$) is a main pathological hallmark of the disease,[4] and oligomers seeded early in this aggregation process are widely considered to be pathogenic.[5,6] A molecular understanding of the factors that regulate Aβ production is thus crucial for combatting the disease.[7] Aβ peptides derive from the sequential cleavage of the amyloid precursor protein by first β-secretase,[8−10] generating C-terminal fragments with 99 amino acids (C99), which are then cleaved by γ-secretase[11,12] to produce Aβ peptides of different lengths (37−43). The formation occurs directly in the membrane, and the lipid−protein interactions thus affect the length, chemical properties, and aggregation tendency of the Aβ peptides.[13−16] The longer $Aβ_{42}$ and $Aβ_{43}$ isoforms are highly aggregation-prone and more toxic in cell cultures.[17] Their involvement in the disease[18] is supported by mutations in presenilin[7] isoforms PSEN1 and PSEN2 that cause early-onset AD; in almost all cases, these mutations increase the ratio of $Aβ_{42}/Aβ_{40}$ peptide isoforms produced by γ-secretase,[19,20] and this ratio is larger for more severe early-onset mutations.[21] γ-secretase contains four subunits: Presenilin is the catalytic subunit, whereas nicastrin, anterior pharynx-defective 1, and presenilin enhancer 2[22−24] play important roles in guiding the C99 substrate entry and exit.[11,12]

Received: August 28, 2018
Accepted: December 10, 2018
Published: December 24, 2018

DOI: 10.1021/acsomega.8b02196
ACS Omega 2018, 3, 18078−18088

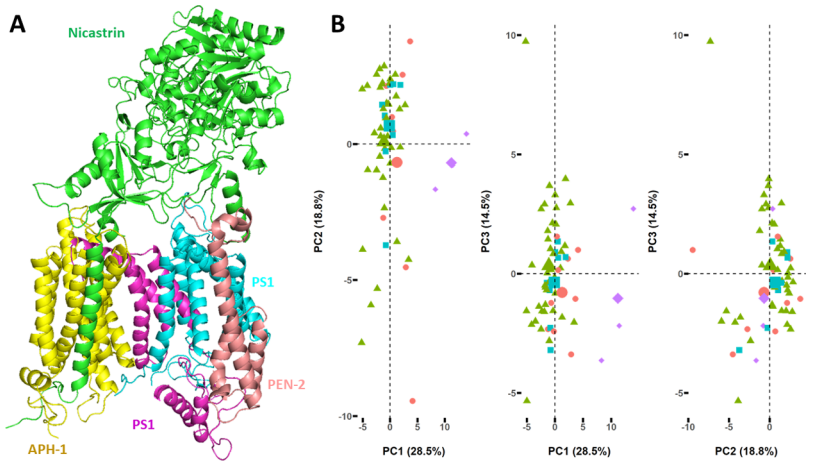

Figure 1. (A) Structure of the semiopen state of γ-secretase with the four subunits nicastrin (green), PS1 (cyan and magenta), APH-1 (yellow), and PEN-2 (pink) used in this work. (B) Score plot showing the first three principal components (PCs). The green triangles represent modulators with EC_{50} < 100 nM; blue squares represent modulators with 100 nM < EC_{50} < 500 nM; red dots represent modulators with 500 nM < EC_{50} < 10 000 nM; and purple diamonds represent modulators with EC_{50} > 10 000 nM. The bigger size indicates that more than one modulator has the same PC coordinates.

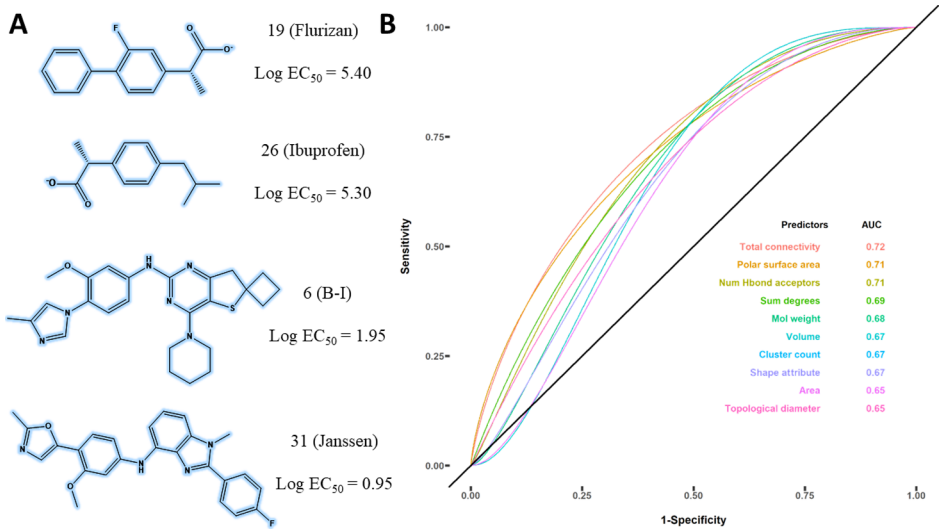

Figure 2. (A) Representative compounds from the GSL60 data set (for a complete list, see Supporting Information). (B) ROC analysis for using the descriptors to distinguish modulators with an EC_{50} cutoff of 100 nM. The figure shows the ROC curves of the top 10 descriptors (AUC = area under the curve).

Direct nonselective inhibition of the protein complex causes side effects which are widely thought to be due to the unwanted inhibition because more than 90 substrates are cleaved by the enzyme complex, including the important notch receptor.[25−27] Alternatively, there is increasing evidence that the reduction in shorter $A\beta_{40}$ may cause a loss of function of this peptide that could also cause side effects.[28] Consequently, focus has moved toward γ-secretase modulators.[29] These compounds preferentially lower $A\beta_{42}$ production without interfering with the cleavage of the other substrates by γ-secretase as they supposedly interact with γ-secretase via multiple allosteric binding sites.[7,30] They tend to favor the production of shorter $A\beta$ peptides, most commonly $A\beta_{38}$,[31,32] and Notch signaling is supposedly not affected by them.[33] The γ-secretase modulators are quite structurally diverse but can be crudely divided into at least three groups.[34−37] The first generation consists of derivatives of nonsteroidal anti-inflammatory drugs (NSAID). These modulators reduce $A\beta_{42}$ and increase production of shorter peptides such as $A\beta_{38}$ through allosteric modification of the interaction between the presenilin catalytic site and C99. Second-generation modulators are structurally diverse and commonly exhibit stronger potency and bioavailability. The third group consists of natural products whose efficiency and safety may vary greatly.[2]

To date, the molecular mechanism that enables γ-secretase modulators to change the $A\beta$ production remains unclear. Given their importance, it seems necessary to understand how these molecules work, which chemical properties that make them function, and how they can be rationally optimized for increased potency. Quantitative structure−activity relationships (QSARs) are state-of-the-art tools for understanding these molecular mechanisms and predicting potency. Very few QSAR studies[38,39] have been directed toward γ-secretase modulators, presumably because the molecular mechanism of modulation is more complex and depends on multiple modulatory sites on the protein surface, whereas classical

DOI: 10.1021/acsomega.8b02196
ACS Omega 2018, 3, 18078−18088

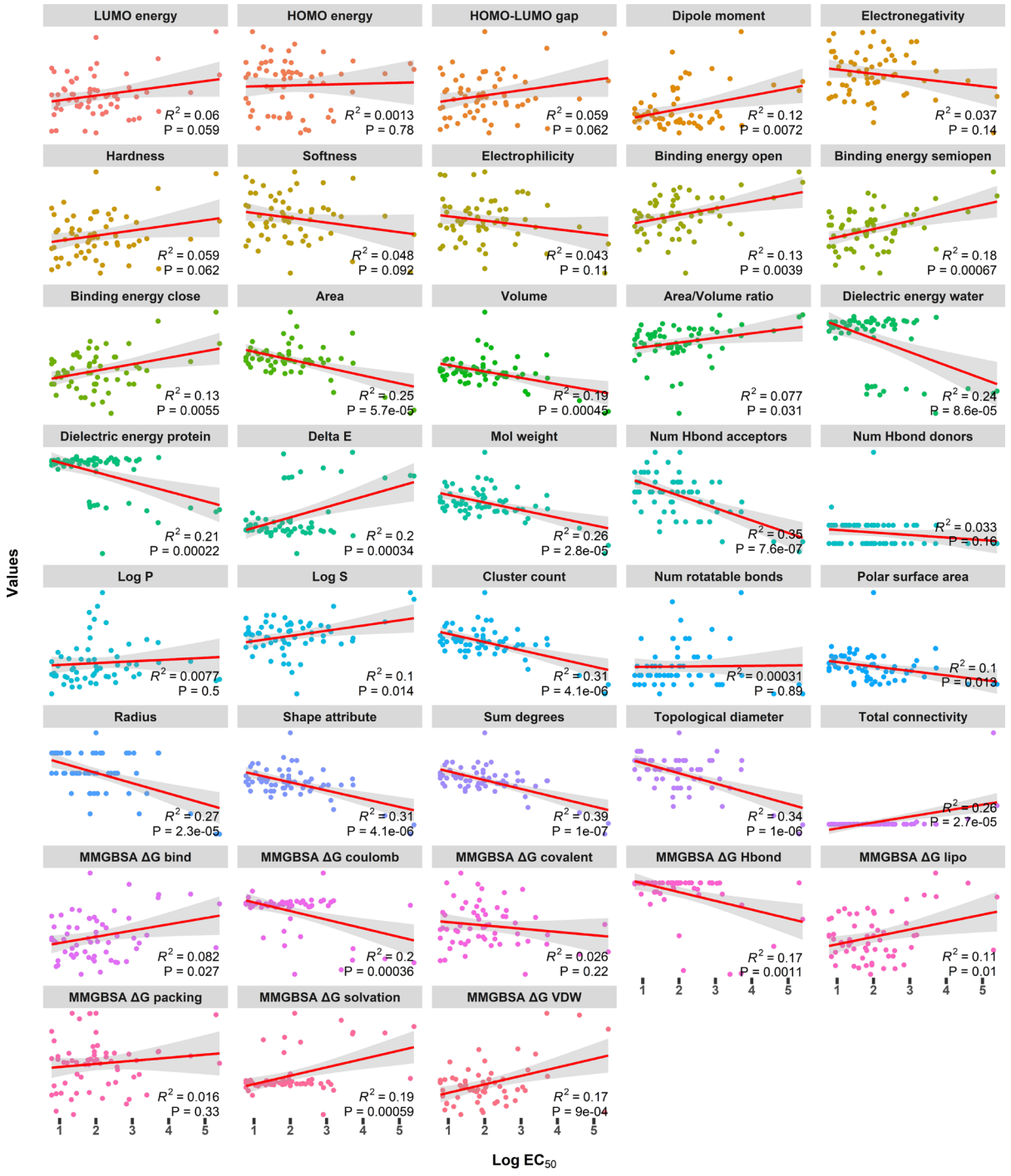

Figure 3. Linear relationship between log EC_{50} values and the numerical values of the calculated chemical properties of the modulators.

inhibitor models can rely on binding to only the active site of the enzyme.

In this work, we compiled a diverse, curated data set of γ-secretase ligands and used a wide suite of regression- and machine-learning methods to build the first accurate QSAR models of γ-secretase modulation, based on quantum mechanical properties of the molecules, binding energies, and their physical components. The models were subject to randomized 10-fold internal as well as explicit external validation. We applied the most complete previously established full-atom γ-secretase structure which obeys all available experimental structural constraints and was equilibrated by 500 ns of molecular dynamics (MD) simulations.[40] The active semi-open state of this protein is shown in Figure 1A. This structure importantly includes all helix side chains, loops, the maturation cleavage into N- and C-terminal fragments required for activity, a membrane, and other features missing in the cryo-electron microscopy structures.[41] Using this modeling approach, we find that strong versus weak modulatory effects can be described by only four descriptors, providing a simple molecular recipe for developing new modulators for the potential treatment of AD.

DOI: 10.1021/acsomega.8b02196
ACS Omega 2018, 3, 18078−18088

Table 1. Evaluation Metrics (R^2, Adjusted R^2, and Root-Mean-Squared Error for the Training Data Set, Test Data Set, and the Whole Data Set) of the 10 Methods Used for Building the QSAR Models[a,b]

method	adj.R^2 (train)	RMSE (train)	R^2 (train)	adj.R^2 (test)	RMSE (test)	R^2 (test)	adj.R^2 (both)	RMSE (both)	R^2 (both)	# descriptors
nnet	0.56	0.66	0.56	0.47	0.70	0.56	0.59	0.65	0.61	4
glmnet	0.51	0.71	0.54	0.41	0.74	0.51	0.54	0.69	0.57	4
lm	0.51	0.71	0.54	0.41	0.73	0.51	0.54	0.68	0.57	4
lassoRMSE	0.52	0.71	0.54	0.41	0.75	0.50	0.54	0.69	0.57	3.7
glmStepAIC	0.50	0.75	0.53	0.37	0.76	0.48	0.52	0.69	0.55	4
pls	0.45	0.70	0.56	0.37	0.77	0.48	0.49	0.72	0.52	4
rfRFE	0.87	0.73	0.51	0.39	0.78	0.48	0.70	0.59	0.71	3.4
rf	0.89	0.76	0.49	0.35	0.78	0.46	0.69	0.57	0.72	4
svmRFE	0.55	0.77	0.54	0.27	0.88	0.38	0.48	0.78	0.51	3.6
svmRadial	0.68	0.77	0.52	0.20	0.87	0.34	0.53	0.68	0.56	4

[a]The four descriptors are the number of hydrogen-bond acceptor sites (N_H), the sum of degrees (S_D), the solvation energy in water (E_{sol}), and the binding free energy to γ-secretase (ΔG_{bind}). [b]nnet = Neural network; glmnet = elastic net regression; lm = multiple linear regression; lassoRMSE = lasso regression; glmStepAIC = generalized linear model with stepwise feature selection; pls = partial least-squares regression; rfRFE = random forest with recursive feature elimination; rf = random forest; svmRFE = support vector machine with recursive feature elimination; and svmRadial = support vector machine using radial functions.

RESULTS AND DISCUSSION

Descriptor Classification and Principal Component Analysis. As the first part of our analysis, we removed the noninformative and zero-variation descriptors, leaving 38 meaningful descriptors as shown in the Supporting Information (XLSX file). Highly correlated descriptors ($R^2 > 0.9$) were not included simultaneously. In general, only clearly informative and meaningful, nonredundant descriptors should be used to build a prediction model. For the descriptor selection, we first performed principal component analysis with the data scaled to zero mean and unit variance; the resulting score plot is shown in Figure 1B. The first three PCs explain 61.8% of the total variation, with the PC1, PC2, and PC3 accounting for 28.5, 18.8, and 14.5%, respectively. The points are colored according to the EC_{50} values. The score plots clearly indicate a good separation of the modulators with high EC_{50} values (purple diamonds). However, Figure 1B exhibits less effective separation for the first three PCs for other modulators, indicating the challenge of modeling very potent modulators. Examples of weak and strong modulators are shown in Figure 2A.

To further analyze this, cluster analysis based on Euclidian distance was performed based on the used descriptors. The dendrogram and associated heat map are shown in Figure S1 (Supporting Information). In general, two main clusters were found and the modulators with high EC_{50} values were grouped within the same cluster, in agreement with the principal component analysis (PCA) results. The individual loading plots are shown in the Supporting Information (Figures S2–S4). PC1 is more positively correlated with the binding free energy (ΔG_{bind}) and to log EC_{50} and negatively correlated with the sum of the degrees (S_D), which describes the complexity of the ligand. PC2 is mainly characterized by the Cosmo solvation energy (dielectric energy in water, E_{sol}) and the number of rotatable bonds. On the basis of the PCA analysis, the most promising 10 descriptors were selected for further QSAR modeling. These selected descriptors cannot separate the modulators with relatively low EC_{50} values but may be capable of predicting whether a prospective modulator will be potent or not.

Descriptor Selection Using Different Methods. The PCA led us to attempt to reduce the complexity of the QSAR models. To this end, receiver operating characteristic (ROC) curve analysis (Figure 2B) was applied to the data set. For the binary classification using the ROC curve analysis, the EC_{50} value of 100 nM was used as a cutoff and the descriptors were used as predictors. Figure 2B lists the top 10 descriptors according to the obtained AUC values. If the descriptor can perfectly separate the modulators, the area under the ROC curve equals 1. As can be seen from Figure 2B, the total connectivity was the best descriptor (AUC of 0.72) for separating the modulators using a cutoff value of 100 nM, followed by polar surface area (AUC of 0.71) and the number of hydrogen-bond acceptor sites of the drug N_H (AUC of 0.71). The top 10 descriptors from this analysis were selected for further modeling.

Another approach, random forest, may improve variable selection. This backward selection method quantifies the relevance of the descriptors based on importance as shown in Figure S5 (Supporting Information). The total connectivity again ranked highly for predicting the log EC_{50} values. We found good consensus between the ROC analysis and the random forest method, as 6 of the top 10 descriptors selected by ROC analysis also entered the top 10 proposed from random forest optimization; the four additional descriptors were also considered for building QSAR models.

The linear relationship between log EC_{50} and the studied descriptors was determined, and the results are shown in Figure 3. We were surprised to find that some descriptors (such as S_D) showed some linear relationships with R^2 up to 0.39 ($p < 0.001$). On the basis of the linear regression and the linear relationship in Figure 3, 10 additional descriptors were considered. With these diverse selected descriptors as the starting point, 4 data sets were obtained with 10 descriptors each. Each time, four descriptors were used for QSAR modeling. In total, 840 test data sets were produced in this way and subsequently used to construct predictive QSAR models. Highly correlated descriptors ($R^2 > 0.9$) were reduced to only one to avoid overfitting.

Neural Network-Optimized QSAR Model of EC_{50}. The summary of the best regression method performance for all of the obtained models based on the evaluation metrics is shown in Table S3 (Supporting Information). As seen from Table S3, the performance of the obtained models vary a lot, and most R^2 values were quite low as expected, indicating the challenge of describing the experimentally observed activity of these

DOI: 10.1021/acsomega.8b02196
ACS Omega 2018, 3, 18078−18088

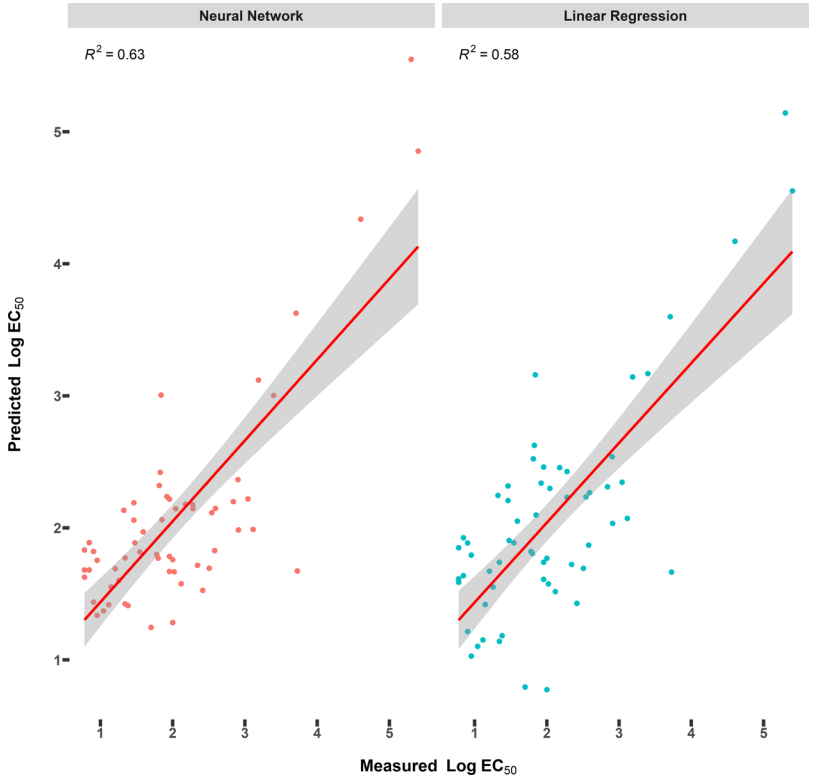

Figure 4. Linear relationship between the measured and predicted log EC_{50} values based on the neural network model (left panel) and multiple linear regression model (right panel).

diverse compounds. On the basis of R^2 and root mean square error (RMSE) values, four descriptors, N_H, S_D, the solvation energy of the drug in water (E_{sol}), and ΔG_{bind} computed by AutoDock Vina showed the best combined ability to describe the log EC_{50} values. The evaluation metrics of all applied methods for these four descriptors are summarized in Table 1. Neural network optimization was most capable of fitting the descriptors to predict log EC_{50}, with R^2 = 0.61 and adjusted R^2 = 0.59, respectively, followed by elastic net regression and multiple linear regression. The applied neural network model is shown in Figure S6 of the Supporting Information. The model has four input-layer neurons equal to the used descriptors and five hidden-layer neurons and a single output-layer neuron. The networks were trained using the Broyden−Fletcher−Goldfarb Shanno algorithm, and decay values of 0, 0.001, and 0.1 were used to avoid overfitting.[42]

To interpret the neural network models, the coefficients of each layer can be obtained as shown in Table S4 of the Supporting Information. We found that ΔG_{bind} of the drug to the protein has substantial contributions to the third and fifth hidden-layer neurons with coefficients of 1.11 and 1.12, respectively. As hidden-layer neurons had high contribution to the out-layer neuron, we conclude that ΔG_{bind}, as measured by AutoDock Vina calculation on the semiopen structure, contributes substantially to the observed log EC_{50} values. The final performance of the neural network model is shown in Figure 4.

Explicit external validation of our models was carried out using 10 additional randomly selected modulators not part of our GSL60 data set but with a similar chemical structure and within the same range of log EC_{50}. The results of this external validation are shown in Figure S7. Although R^2 values were reduced to 0.33−0.34, considering the complexity of the modulatory effect and the high diversity of the data set, this performance is encouraging. As shown in Table 1, the multilinear regression method also produced good performance as indicated by R^2 and RMSE values. The finding that four-descriptor models can describe and pseudopredict high versus low log EC_{50} values is of significance to our future efforts in understanding γ-secretase and its modulation for therapeutic purposes.

Chemical Interpretation of the Obtained Modulation Model. To understand the molecular basis of modulation, the multilinear regression model was also interpreted in detail. The performance of the model is shown in Figure 4 (right panel) with the external validation shown in Figure S7. Because normalization was used during modeling, to obtain the coefficients corresponding to the original data set, the scaled coefficients were multiplied by a scaling factor giving the model of eq 1

$$\log EC_{50} = 6.38 - 0.14N_H - 0.02S_D - 0.43E_{sol} + 0.24\Delta G_{bind} \quad (1)$$

The solvation energy in water had the strongest contribution to the trend prediction (its removal reduces R^2 by 0.1), whereas the other three terms are of similar importance. In terms of their contribution to the modeled log EC_{50} value, their relative importance is roughly 0.9, 1.4, 0.6, and 2.2, as measured by their effect on the mean signed error of predicted log EC_{50} when removing the term. The identified descriptors were not highly correlated, indicating that they are informative in different ways.

Because both energy terms are computed as negative numbers (with more negative meaning stronger binding energy to water or protein, respectively), the last two terms

DOI: 10.1021/acsomega.8b02196
ACS Omega 2018, 3, 18078−18088

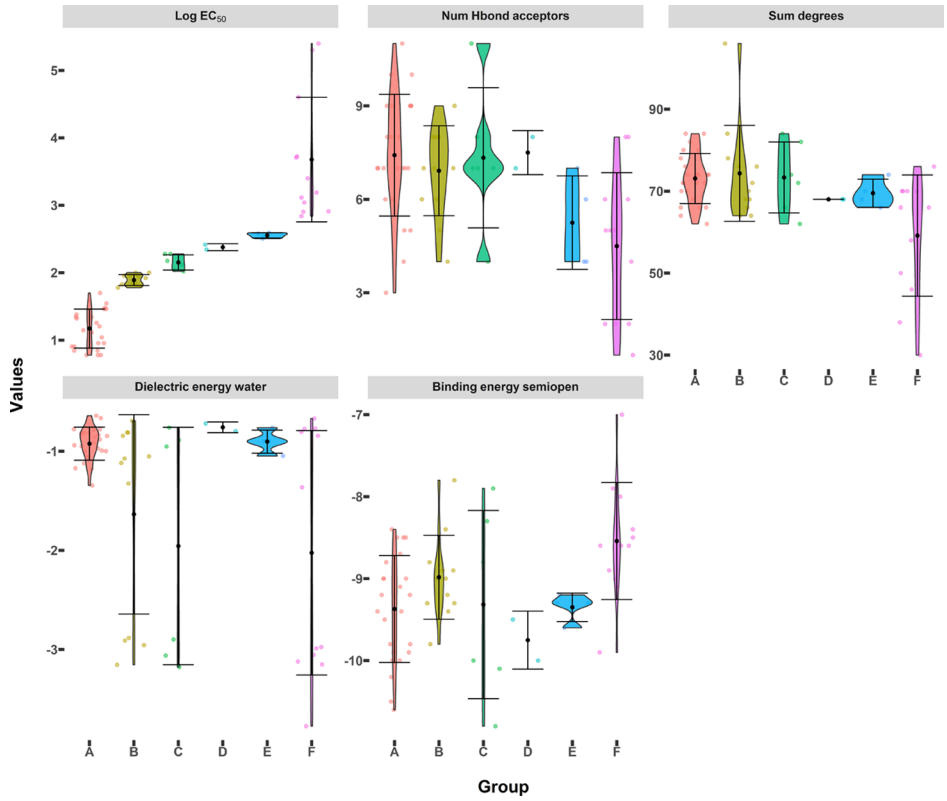

Figure 5. Distribution of values of log EC_{50} and of the four best descriptors of log EC_{50} divided into five groups of modulators: group A has EC_{50} < 50 nM; group B has 50 nM < EC_{50} < 100 nM; group C has 100 nM < EC_{50} < 200 nM; group D has 200 nM < EC_{50} < 300 nM; group E has 300 nM < EC_{50} < 500 nM; and group F has EC_{50} > 500 nM. Averages are shown as black dots and standard deviations are shown as bars. Points have been distributed on the horizontal axis for clarity.

essentially represent the dehydration penalty and the protein−ligand binding energy contributions to the potency of the modulator, that is, the two terms describe the net strength of the ligand−protein interaction. The signs are thus directly physically meaningful and the two terms compete to affect the EC_{50} value.

Stronger association of the modulator with the protein due to these two terms contributes significantly to explaining experimental EC_{50} values. In contrast, any molecular mechanism that explains how these compounds selectively lower $A\beta_{42}$ peptide production is, at this point, elusive. However, recent work suggests that two distinct modulators change the conformation state of γ-secretase explicitly.[43] Our results indicate that the structural requirements for γ-secretase modulation differ widely for the 60 studied compounds, which is probably due to the presence of multiple distinct modulatory sites.[44] This complication makes the importance of model (1) more evident because it reproduces log EC_{50} without any use of information of these variable modulatory binding sites but only general nonspecific binding information as well as information relating to the interaction types of the ligand with the protein surface.

To understand the modulatory effect in more detail, we divided the modulators into six groups based on their EC_{50} values, and the four chemical properties obtained from QSAR modeling were displayed for each group (Figure 5). There is no simple correlation between the binding energy and the observed activity, and the binding energy varies substantially among the groups. The residues in the binding sites also contribute to the interactions and volume of the binding pocket.[45] In addition to the two energy terms that compete to produce the overall drug affinity, the number of hydrogen bond acceptor sites (N_H) in the compound contributes consistently to lowering log EC_{50}. The ROC analysis showed the importance of this descriptor for distinguishing modulators with low EC_{50} values (100 nM). Despite the substantial variation among the groups of compounds, it is notable that modulators with lower EC_{50} values tend to have more hydrogen-bond acceptor sites.

Larger molecules, all else being equal, are more capable of affecting the conformational state of a protein and will also, again all else being equal, bind more strongly. Accordingly, the number of hydrogen bond acceptors is a prominent feature in many pharmacophore-based QSAR models.[46] Combining this with the insight from the dehydration penalty (the dielectric energy in eq 1), we conclude that potent γ-secretase modulators should be relatively hydrophobic while still possessing lone-pair electrons on heteroatoms to modulate γ-secretase efficiently. The importance of the hydrogen-bond acceptors has been addressed in previous attempts to develop new γ-secretase modulators.[47] Previous work has shown that some modulators interact with γ-secretase through hydrogen bonds and $\pi-\pi$ interactions.[48]

Solvation effects contribute substantially to the variations in binding energy between relatively similar ligands.[49] We were intrigued that the dehydration penalty, as estimated by the Cosmo solvation energy of the modulators in water, contributes substantially to the measured EC_{50}. Despite being a QM/density functional theory (DFT) calculation, it can be performed routinely for many compounds using the

DOI: 10.1021/acsomega.8b02196
ACS Omega 2018, 3, 18078−18088

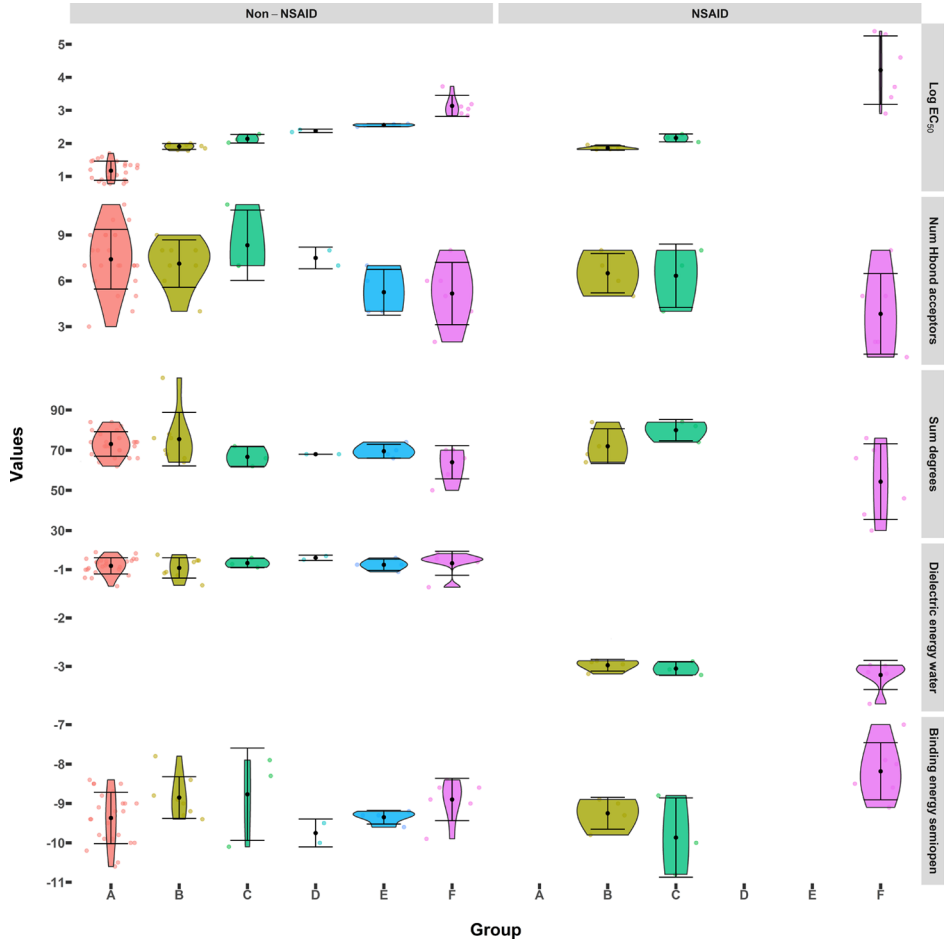

Figure 6. Distribution of values of log EC_{50} and of the best descriptors of log EC_{50} divided into groups as in Figure 5. Averages are shown as black dots and standard deviations shown as bars. Points have been distributed on the horizontal axis for clarity.

applied procedure. As for the binding energy, Figure 5, there was no simple relationship between the solvation energy and the observed log EC_{50}. It is only in the complete four-descriptor model optimized by the neural network that the relative importance of these two competing energy terms becomes apparent. Figure S8 shows that there are two major groups in terms of the solvation energy, reflecting well the categorization into hydrophobic and hydrophilic compounds.

S_D of the compound was also found to be an important descriptor of EC_{50}. This property is defined as the sum of all bonds between nonhydrogen atoms. Thus, a high value represents a weakly saturated, compact molecule. It is highly correlated with the shape attribute (0.99) and molecular weight (0.95). This measure of the complexity of the ligand adds important predictive value to the model (Figure 5), as modulators with high EC_{50} values in group F (EC_{50} > 500 nM) have relatively low complexity.

In summary, the four descriptors have meaningful interpretations that probably relate to the real, still not fully understood C99 processing mechanism of γ-secretase. It is also notable that the model produced, eq 1, has the form of a nonspecific general contribution to a high log EC_{50} for any compound but subsequently reduced by the four terms separately, considering the sign conventions of the last two energy terms discussed above. In other words, any rational prediction would start with log EC_{50} ~6.4 and then work downward by optimizing the protein−modulator interactions, the shape, and reducing the dehydration penalty. The most successful modulators only reach the nanomolar range by such a combination of strategies.

We further analyzed the chemical property distribution of the modulators based on their division into NSAIDs and non-NSAIDs; the results are shown in Figure 6. The non-NSAID modulators in the data set were generally more efficient, with lower EC_{50} values. The modulators with EC_{50} values <50 nM were all non-NSAID modulators. For N_H and S_D, these results are in accordance with the overall analysis shown in Figure 6. Notably, as shown in Figure 6, E_{sol} values for the non-NSAID modulators were significantly higher than those for the NSAID modulators. The NSAID modulators with very high EC_{50} values bind more weakly to γ-secretase than the other investigated modulators (Figure 6). In a recent study, γ-secretase modulators were found to have a synergistic effect toward their modulatory activity for non-NSAID and NSAID combinations, indicating that these two types of γ-secretase modulators may target different binding sites in the protein.[50]

Implications for the Molecular Mechanism of Familial AD. Previous studies suggest that γ-secretase should bind to its natural substrate C99 long enough to let the substrate be cleaved repeatedly.[51] The reaction kinetics are affected by both enzyme and substrate as seen from mutation studies.[52] The non-NSAID γ-secretase modulators induce conformational changes of γ-secretase that affect the production of $A\beta_{42}$ peptides.[53] These findings are consistent with full-atom MD

DOI: 10.1021/acsomega.8b02196
ACS Omega 2018, 3, 18078−18088

simulations showing that the binding affinity between the semiopen state of γ-secretase and C99 increases the retention time and thereby the extent of trimming within the protein complex, while the open state binds C99 less well and accordingly releases it after a relatively short time (the FIST model).[40] Thus, we have a complete mechanistic working model of γ-secretase that explains both the effect of modulators and the impact of PSEN1 mutations that cause early-onset AD, either favoring or disfavoring the compact stability of the protein complex to favor the open conformation state that is less catalytically proficient and releases Aβ earlier at longer lengths.[54,55] We refer to this as the FIST (Fit, Stay, Trim) mechanism where the trimming of C99 is controlled by its adequate "squeezing".

CONCLUSIONS

There is urgent need to understand the molecular basis for modulation of γ-secretase to develop new therapies that modulate the activity of this enzyme complex. Many γ-secretase modulators reduce $A\beta_{42}$ production and increase $A\beta_{38}$ peptides,[31,36] but there is no molecular mechanism that can explain their function. One of the most haunting questions is why so many diverse molecules, including molecules such as ibuprofen, selectively lower the $A\beta_{42}$ production.

We explored the activity of 60 of the most known modulators with the help of structural and chemical descriptors. Our compiled data set (GSL60) contains structurally and chemically diverse γ-secretase modulators with a wide range of EC_{50} values. Using neural network optimization, we have identified a chemically meaningful model based on only four descriptors, which explains most of the variation in the observed log EC_{50}. The four descriptors are the number of hydrogen acceptor sites, the complexity of the drug measured by S_D, the desolvation energy penalty measured by the solvation energy of the drug, and the binding free energy to the protein. The model reveals the major importance of strong, nonspecific binding to multiple modulatory sites, mainly by favoring large complex molecules with a small dehydration penalty, many hydrogen-bond acceptor sites, and a favorable free energy of binding to the protein. We envision that our model can be used for virtual screening of new γ-secretase modulator candidates.

Our FIST (Fit, Stay, Trim) mechanism of γ-secretase rationalizes the outcome of both modulators and pathogenic PSEN1 mutations working to opposite effects: modulators favor tight substrate association and increase the retention time of C99, whereas pathogenic PSEN1 mutations favor the open state of the protein and shorten the retention time of C99 to increase the average length of the produced Aβ peptides. Accordingly, our model suggests that many molecules can modulate cleavage simply by contributing their binding energy to stabilize the compact ternary complex with C99.

Our mechanism requires further experimental support. It only captures some properties that correlate with experimental EC_{50} for 60 drugs, without actually knowing the modulatory sites themselves. Also, the diversity of the data set reduces the explanatory power for low-affinity drugs. This however also shows that experimental claims based on a few modulators may be misleading as the modulators and their function via multiple descriptors are chemically diverse, a fact that justifies our computational approach, which will be expanded to include more compounds and more physiologically relevant chemical models in the future.

COMPUTATIONAL METHODS

GSL60 γ-Secretase Modulator Data Set. The γ-secretase modulators were selected based on the diversity in structure and EC_{50} based on two extensive reviews, which covered most key patents and articles published in this field until 2016.[35,36] The other compounds were added according to the papers published by different groups in 2016 and 2017.[47,56−59] The final curated data set (GSL60) contains 60 compounds from 25 research groups with EC_{50} values ranging from 6 nM to 250 μM, that is, it spreads well the range of values with representatives of all major compound classes. Out of 60 modulators, 13 are NSAIDs, 46 are non-NSAIDs, and 1 (compound **53**) is a natural product included as a control as these are too diverse for modeling with limited data available. Some examples include the NSAIDs ibuprofen (compound **26** in the data base) and Tarenflurbil (Flurizan, compound **19**) and three aminothiazoles (compounds **57**−**59**), which have shown promising activity in the nanomolar range recently.[60] Compounds were selected broadly from major companies such as pyridopyrazine-1,6-diones and amides from Pfizer, triazole derivatives from Merck, carboxylic acids and anilines from GSK and Janssen, thienopyrimidines from Boehringer-Ingelheim (B-I), and several anilines and tricyclic amines from Bristol-Meyers Squibb. Because most of the developments in γ-secretase modulators are relatively recent, most of the compounds were published after 2011. A summary of the data set is given in the Supporting Information, Table S1.

To build the molecules of the data set for further processing, the 3D coordinates for each compound were individually searched and downloaded from the PubChem database.[61] Structures that could not be found in PubChem were generated by the MarvinSketch tool. Then, all structures were optimized at pH 7.0 using the LigPrep tool of the Schrödinger Suite with the OPLS3 force field, which was specifically developed for good accuracy when applied to drug-like molecules.[62] The molecular structures were subsequently used for calculation of the QSAR descriptor values.

Calculation of Quantum Mechanical Descriptors. All quantum mechanical calculations presented in this study were performed using DFT with the Turbomole 7.0 software. To speed up calculation, we used the resolution of identity approximation for geometry optimization of all 60 molecules, which does not affect the obtained equilibrium structure but accelerates convergence.[63] We used the B3LYP functional and the 6-31G(d,p) basis set for geometry optimization. Solvent effects were included using the COSMO model.[64] Specifically, we hypothesized that the difference between the COSMO solvation energy of a water- and a protein-like environment might provide an estimate of the nonspecific binding of the modulators to the protein. Thus, dielectric constants of 4 and 80 were both used for computing E_{sol}. In addition, Koopmans' theorem was applied to the DFT Kohn−Sham orbital energies[65] to compute quantum mechanical descriptors such as the electronegativity, chemical potential, ionization potential, electron affinity, chemical hardness and softness, and electrophilicity index.

Calculation of the Binding Free Energy. The free energy of binding the modulators to γ-secretase (ΔG_{bind}) was calculated using AutoDock Vina.[66] The structure used for docking was previously established by multitemplate homology modeling and relaxed by MD simulations for 500 ns.[40] Multiseed MD simulations revealed three distinct conforma-

DOI: 10.1021/acsomega.8b02196
ACS Omega 2018, 3, 18078−18088

tional states of γ-secretase that differ in the access to the cleavage site flanked by helices 2, 3, and 6.[40] We identified the semiopen state as having optimal contacts and the longest residence time for C99, and thus, we suggested that this is the normal innocent form of the protein complex that produces the shortest Aβ isomers.[40] In contrast, mutations in PSEN1 commonly reduce hydrophobic packing and protein stability in a way that favors the open conformation state and correlates directly with the clinical severity of the mutations. The open state has shorter residence time of C99 because of nonoptimal substrate−protein interactions and thus releases Aβ peptides with longer lengths, according to our model, which is referred to as the FIST (Fit, Stay, Trim) mechanism below.[54,55] As this open state is probably characteristic of PSEN1 mutants, we used the semiopen state here as it represents the dominating state of the wild-type protein.

The full protein complex structure of the semiopen state was first repaired by FoldX[67] through RepairPDB function to remove crashes and then processed by MGL tools and converted to PDBQT format. DFT-optimized structures of the modulators were used and converted to PDBQT format using the Open Babel software with the default setup.[68] A grid box size of 70 × 60 × 80 Å was used with the whole transmembrane region as the target for docking. The top scores for all investigated modulators were used as estimates of the binding energy to γ-secretase.

Topological and MMGBSA Energy Descriptors. All topological descriptors were calculated based on the DFT-optimized structures, by using the Chem3D 16.0 software. The MMGBSA descriptors were calculated using Prime of the Schrödinger Suite and the OPLS3 force field[62] applied to the semiopen structure. The initial coordinates of the protein modulator complexes were obtained from Glide docking using standard precision and used as input during the MMGBSA calculations.[69,70]

QSAR Models. After collecting all descriptors, the data set was normalized and divided into a training data set (60%) and test data set (40%). To avoid bias, 10-fold repeated cross-validation and Y randomization for the best model were applied during the analysis. The following 10 methods were used to ensure adequate optimization of the QSAR models: multiple linear regression (lm), partial least-squares regression (pls), generalized linear model with stepwise feature selection (glmStepAIC), elastic net regression (glmnet), lasso regression (lassoRMSE), random forest (rf), random forest recursive feature elimination (rfRFE), support vector machine using radial function (svmRadial), support vector machine recursive feature elimination (svmRFE), and neural networks (nnet). These methods were applied using a wrapper package called RRegrs in R,[42] using the standard parameters. For the time-consuming methods svmRFE and rfRFE, 3- and 5-fold cross-validation with one repeat was applied, respectively. The selection of the models was based on the obtained R^2 and RMSE.

Finally, the models were subject to explicit external validation using a distinct secondary data set of 10 modulators. These 10 modulators differ from the 60 molecules of the GSL60 data set and were randomly selected among alternative modulators with similar log EC_{50} range. Details on these 10 additional modulators used for external validation are provided in Supporting Information, Table S2.

■ ASSOCIATED CONTENT

Supporting Information

The Supporting Information is available free of charge on the ACS Publications website at DOI: 10.1021/acsomega.8b02196.

Details on the full GSL60 data set of the compounds; external validation data set of the compounds; performance of all final models with the best optimization method; coefficients of the neural network model; heatmap; loading plots of the principle component analysis; descriptor importance obtained through random forest; neural network model; performance of the external validation; and value distribution of the descriptors used (PDF)

Details and classification of descriptors (XLSX)

■ AUTHOR INFORMATION

Corresponding Author

*E-mail: kpj@kemi.dtu.dk (K.P.K.).

ORCID

Kasper P. Kepp: 0000-0002-6754-7348

Notes

The authors declare no competing financial interest.

■ ACKNOWLEDGMENTS

The Danish Council for Independent Research|Natural Sciences (DFF), grant case 7016-00079B, is acknowledged for supporting this work.

■ REFERENCES

(1) Lai, R.; Albala, B.; Kaplow, J. M.; Aluri, J.; Yen, M.; Satlin, A. First-in-human study of E2609, a novel BACE1 inhibitor, demonstrates prolonged reductions in plasma beta-amyloid levels after single dosing. *Alzheimer's Dementia* **2012**, *8*, P96.

(2) Kumar, D.; Ganeshpurkar, A.; Kumar, D.; Modi, G.; Gupta, S. K.; Singh, S. K. Secretase inhibitors for the treatment of Alzheimer's disease: Long road ahead. *Eur. J. Med. Chem.* **2018**, *148*, 436−452.

(3) Graham, W. V.; Bonito-Oliva, A.; Sakmar, T. P. Update on Alzheimer's Disease Therapy and Prevention Strategies. *Annu. Rev. Med.* **2017**, *68*, 413−430.

(4) Kalback, W.; Watson, M. D.; Kokjohn, T. A.; Kuo, Y.-M.; Weiss, N.; Luehrs, D. C.; Lopez, J.; Brune, D.; Sisodia, S. S.; Staufenbiel, M.; et al. APP Transgenic Mice Tg2576 Accumulate Aβ Peptides That Are Distinct from the Chemically Modified and Insoluble Peptides Deposited in Alzheimer's Disease Senile Plaques†. *Biochemistry* **2002**, *41*, 922−928.

(5) Musiek, E. S.; Holtzman, D. M. Three dimensions of the amyloid hypothesis: time, space and "wingmen". *Nat. Neurosci.* **2015**, *18*, 800−806.

(6) Sowade, R. F.; Jahn, T. R. Seed-induced acceleration of amyloid-β mediated neurotoxicity in vivo. *Nat. Commun.* **2017**, *8*, 512.

(7) Lessard, C. B.; Cottrell, B. A.; Maruyama, H.; Suresh, S.; Golde, T. E.; Koo, E. H. γ-Secretase Modulators and APH1 Isoforms Modulate γ-Secretase Cleavage but Not Position of ε-Cleavage of the Amyloid Precursor Protein (APP). *PLoS One* **2015**, *10*, No. e0144758.

(8) Yan, R.; Bienkowski, M. J.; Shuck, M. E.; Miao, H.; Tory, M. C.; Pauley, A. M.; Brashler, J. R.; Stratman, N. C.; Mathews, W. R.; Buhl, A. E.; et al. Membrane-anchored aspartyl protease with Alzheimer's disease β-secretase activity. *Nature* **1999**, *402*, 533−537.

(9) Sinha, S.; Anderson, J. P.; Barbour, R.; Basi, G. S.; Caccavello, R.; Davis, D.; Doan, M.; Dovey, H. F.; Frigon, N.; Hong, J.; et al. Purification and cloning of amyloid precursor protein β-secretase from human brain. *Nature* **1999**, *402*, 537−540.

DOI: 10.1021/acsomega.8b02196
ACS Omega 2018, 3, 18078−18088

(10) Vassar, R.; Bennett, B. D.; Babu-Khan, S.; Kahn, S.; Mendiaz, E. A.; Denis, P.; Teplow, D. B.; Ross, S.; Amarante, P.; Loeloff, R.; et al. Beta-Secretase Cleavage of Alzheimer's Amyloid Precursor Protein by the Transmembrane Aspartic Protease BACE. *Science* **1999**, *286*, 735−741.
(11) Kang, J.; Lemaire, H.-G.; Unterbeck, A.; Salbaum, J. M.; Masters, C. L.; Grzeschik, K.-H.; Multhaup, G.; Beyreuther, K.; Müller-Hill, B. The precursor of Alzheimer's disease amyloid A4 protein resembles a cell-surface receptor. *Nature* **1987**, *325*, 733−736.
(12) Koo, E. H.; Kopan, R. Potential role of presenilin-regulated signaling pathways in sporadic neurodegeneration. *Nat. Med.* **2004**, *10*, S26.
(13) Matsumura, N.; Takami, M.; Okochi, M.; Wada-Kakuda, S.; Fujiwara, H.; Tagami, S.; Funamoto, S.; Ihara, Y.; Morishima-Kawashima, M. γ-Secretase Associated with Lipid Rafts. *J. Biol. Chem.* **2013**, *289*, 5109−5121.
(14) Kotler, S. A.; Walsh, P.; Brender, J. R.; Ramamoorthy, A. Differences between amyloid-β aggregation in solution and on the membrane: Insights into elucidation of the mechanistic details of Alzheimer's disease. *Chem. Soc. Rev.* **2014**, *43*, 6692.
(15) Brender, J. R.; Lee, E. L.; Hartman, K.; Wong, P. T.; Ramamoorthy, A.; Steel, D. G.; Gafni, A. Biphasic effects of insulin on islet amyloid polypeptide membrane disruption. *Biophys. J.* **2011**, *100*, 685−692.
(16) Matsuzaki, K. How Do Membranes Initiate Alzheimer's Disease? Formation of Toxic Amyloid Fibrils by the Amyloid β-Protein on Ganglioside Clusters. *Acc. Chem. Res.* **2014**, *47*, 2397−2404.
(17) Selkoe, D. J.; Hardy, J. The amyloid hypothesis of Alzheimer's disease at 25 years. *EMBO Mol. Med.* **2016**, *8*, 595.
(18) Walsh, D. M.; Selkoe, D. J. Deciphering the molecular basis of memory failure in Alzheimer's disease. *Neuron* **2004**, *44*, 181−193.
(19) Borchelt, D. R.; Thinakaran, G.; Eckman, C. B.; Lee, M. K.; Davenport, F.; Ratovitsky, T.; Prada, C.-M.; Kim, G.; Seekins, S.; Yager, D.; et al. Familial Alzheimer's Disease-Linked Presenilin 1 Variants Elevate Aβ1-42/1-40 Ratio In Vitro and In Vivo. *Neuron* **1996**, *17*, 1005−1013.
(20) Scheuner, D.; Eckman, C.; Jensen, M.; Song, X.; Citron, M.; Suzuki, N.; Bird, T. D.; Hardy, J.; Hutton, M.; Kukull, W.; et al. Secreted amyloid β-protein similar to that in the senile plaques of Alzheimer's disease is increased in vivo by the presenilin 1 and 2 and APP mutations linked to familial Alzheimer's disease. *Nat. Med.* **1996**, *2*, 864−870.
(21) Tang, N.; Kepp, K. P. Aβ42/Aβ40 ratios of presenilin 1 mutations correlate with clinical onset of Alzheimer's disease. *J. Alzheimer's Dis.* **2018**, *66*, 939.
(22) De Strooper, B.; Saftig, P.; Craessaerts, K.; Vanderstichele, H.; Guhde, G.; Annaert, W.; Von Figura, K.; Van Leuven, F. Deficiency of presenilin-1 inhibits the normal cleavage of amyloid precursor protein. *Nature* **1998**, *391*, 387−390.
(23) Wolfe, M. S.; Xia, W.; Ostaszewski, B. L.; Diehl, T. S.; Kimberly, W. T.; Selkoe, D. J. Two transmembrane aspartates in presenilin-1 required for presenilin endoproteolysis and γ-secretase activity. *Nature* **1999**, *398*, 513−517.
(24) Sato, T.; Diehl, T. S.; Narayanan, S.; Funamoto, S.; Ihara, Y.; De Strooper, B.; Steiner, H.; Haass, C.; Wolfe, M. S. Active -Secretase Complexes Contain Only One of Each Component. *J. Biol. Chem.* **2007**, *282*, 33985−33993.
(25) Tamayev, R.; D'Adamio, L. Inhibition of γ-secretase worsens memory deficits in a genetically congruous mouse model of Danish dementia. *Mol. Neurodegener.* **2012**, *7*, 19.
(26) Milano, J.; McKay, J.; Dagenais, C.; Foster-Brown, L.; Pognan, F.; Gadient, R.; Jacobs, R. T.; Zacco, A.; Greenberg, B.; Ciaccio, P. J. Modulation of Notch Processing by γ-Secretase Inhibitors Causes Intestinal Goblet Cell Metaplasia and Induction of Genes Known to Specify Gut Secretory Lineage Differentiation. *Toxicol. Sci.* **2004**, *82*, 341−358.
(27) van Es, J. H.; van Gijn, M. E.; Riccio, O.; van den Born, M.; Vooijs, M.; Begthel, H.; Cozijnsen, M.; Robine, S.; Winton, D. J.; Radtke, F.; et al. Notch/γ-secretase inhibition turns proliferative cells in intestinal crypts and adenomas into goblet cells. *Nature* **2005**, *435*, 959−963.
(28) Kepp, K. P. Alzheimer's disease due to loss of function: A new synthesis of the available data. *Prog. Neurobiol.* **2016**, *143*, 36−60.
(29) De Strooper, B.; Chávez Gutiérrez, L. Learning by Failing: Ideas and Concepts to Tackle γ-Secretases in Alzheimer's Disease and Beyond. *Annu. Rev. Pharmacol. Toxicol.* **2015**, *55*, 419−437.
(30) Weggen, S.; Eriksen, J. L.; Sagi, S. A.; Pietrzik, C. U.; Golde, T. E.; Koo, E. H. Aβ42-lowering Nonsteroidal Anti-inflammatory Drugs Preserve Intramembrane Cleavage of the Amyloid Precursor Protein (APP) and ErbB-4 Receptor and Signaling through the APP Intracellular Domain. *J. Biol. Chem.* **2003**, *278*, 30748−30754.
(31) Weggen, S.; Eriksen, J. L.; Das, P.; Sagi, S. A.; Wang, R.; Pietrzik, C. U.; Findlay, K. A.; Smith, T. E.; Murphy, M. P.; Bulter, T.; et al. A subset of NSAIDs lower amyloidogenic Aβ42 independently of cyclooxygenase activity. *Nature* **2001**, *414*, 212−216.
(32) Ohki, Y.; Higo, T.; Uemura, K.; Shimada, N.; Osawa, S.; Berezovska, O.; Yokoshima, S.; Fukuyama, T.; Tomita, T.; Iwatsubo, T. Phenylpiperidine-type γ-secretase modulators target the transmembrane domain 1 of presenilin 1. *EMBO J.* **2011**, *30*, 4815−4824.
(33) Sagi, S. A.; Lessard, C. B.; Winden, K. D.; Maruyama, H.; Koo, J. C.; Weggen, S.; Kukar, T. L.; Golde, T. E.; Koo, E. H. Substrate Sequence Influences γ-Secretase Modulator Activity, Role of the Transmembrane Domain of the Amyloid Precursor Protein. *J. Biol. Chem.* **2011**, *286*, 39794−39803.
(34) Wolf, M. γ-Secretase as a Target for Alzheimers Disease. *Curr. Top. Med. Chem.* **2002**, *2*, 371−383.
(35) Oehlrich, D.; Berthelot, D. J.-C.; Gijsen, H. J. M. γ-Secretase modulators as potential disease modifying anti-Alzheimer' s drugs. *J. Med. Chem.* **2010**, *54*, 669−698.
(36) Bursavich, M. G.; Harrison, B. A.; Blain, J.-F. Gamma Secretase Modulators: New Alzheimer's Drugs on the Horizon? *J. Med. Chem.* **2016**, *59*, 7389−7409.
(37) Borgegard, T.; Juréus, A.; Olsson, F.; Rosqvist, S.; Sabirsh, A.; Rotticci, D.; Paulsen, K.; Klintenberg, R.; Yan, H.; Waldman, M.; et al. First and Second Generation γ-Secretase Modulators (GSMs) Modulate Amyloid-β (Aβ) Peptide Production through Different Mechanisms. *J. Biol. Chem.* **2012**, *287*, 11810−11819.
(38) Hieke, M.; Ness, J.; Steri, R.; Dittrich, M.; Greiner, C.; Werz, O.; Baumann, K.; Schubert-Zsilavecz, M.; Weggen, S.; Zettl, H. Design, Synthesis, and Biological Evaluation of a Novel Class of γ-Secretase Modulators with PPARγ Activity. *J. Med. Chem.* **2010**, *53*, 4691−4700.
(39) Khani, H.; Sepehrifar, M. B.; Yarahmadian, S. An improvement on the prediction power of the 3D-QSAR CoMFA models using a hybrid of statistical and machine learning methods: a case study on γsecretase modulators of Alzheimer's disease. *Med. Chem. Res.* **2017**, *26*, 1184−1200.
(40) Somavarapu, A. K.; Kepp, K. P. Membrane Dynamics of γ-Secretase Provides a Molecular Basis for β-Amyloid Binding and Processing. *ACS Chem. Neurosci.* **2017**, *8*, 2424−2436.
(41) Bai, X.-c.; Yan, C.; Yang, G.; Lu, P.; Ma, D.; Sun, L.; Zhou, R.; Scheres, S. H. W.; Shi, Y. An atomic structure of human γ-secretase. *Nature* **2015**, *525*, 212−217.
(42) Tsiliki, G.; Munteanu, C. R.; Seoane, J. A.; Fernandez-Lozano, C.; Sarimveis, H.; Willighagen, E. L. RRegrs: An R package for computer-aided model selection with multiple regression models. *J. Cheminf.* **2015**, *7*, 46.
(43) Raven, F.; Ward, J. F.; Zoltowska, K. M.; Wan, Y.; Bylykbashi, E.; Miller, S. J.; Shen, X.; Choi, S. H.; Rynearson, K. D.; Berezovska, O.; et al. Soluble Gamma-secretase Modulators Attenuate Alzheimer's β-amyloid Pathology and Induce Conformational Changes in Presenilin 1. *EBioMedicine* **2017**, *24*, 93−101.
(44) Pozdnyakov, N.; Murrey, H. E.; Crump, C. J.; Pettersson, M.; Ballard, T. E.; am Ende, C. W.; Ahn, K.; Li, Y.-M.; Bales, K. R.; Johnson, D. S. γ-Secretase Modulator (GSM) Photoaffinity Probes Reveal Distinct Allosteric Binding Sites on Presenilin. *J. Biol. Chem.* **2013**, *288*, 9710−9720.

DOI: 10.1021/acsomega.8b02196
ACS Omega 2018, 3, 18078−18088

(45) Zettl, H.; Weggen, S.; Schneider, P.; Schneider, G. Exploring the chemical space of γ-secretase modulators. *Trends Pharmacol. Sci.* **2010**, *31*, 402−410.
(46) Gousiadou, C.; Kouskoumvekaki, I. Computational analysis of LOX1 inhibition identifies descriptors responsible for binding selectivity. *ACS Omega* **2018**, *3*, 2261−2272.
(47) Bursavich, M. G.; Harrison, B. A.; Acharya, R.; Costa, D. E.; Freeman, E. A.; Hodgdon, H. E.; Hrdlicka, L. A.; Jin, H.; Kapadnis, S.; Moffit, J. S.; et al. Design, Synthesis, and Evaluation of a Novel Series of Oxadiazine Gamma Secretase Modulators for Familial Alzheimer's Disease. *J. Med. Chem.* **2017**, *60*, 2383−2400.
(48) Tomita, T.; Maruyama, K.; Saido, T. C.; Kume, H.; Shinozaki, K.; Tokuhiro, S.; Capell, A.; Walter, J.; Grunberg, J.; Haass, C.; et al. The presenilin 2 mutation (N141I) linked to familial Alzheimer disease (Volga German families) increases the secretion of amyloid protein ending at the 42nd (or 43rd) residue. *Proc. Natl. Acad. Sci. U.S.A.* **1997**, *94*, 2025−2030.
(49) Mobley, D. L.; Dill, K. A. Binding of Small-Molecule Ligands to Proteins: "What You See" Is Not Always "What You Get". *Structure* **2009**, *17*, 489−498.
(50) Robertson, A. S.; Iben, L. G.; Wei, C.; Meredith, J. E.; Drexler, D. M.; Banks, M.; Vite, G. D.; Olson, R. E.; Thompson, L. A.; Albright, C. F.; et al. Synergistic inhibition of Aβ production by combinations of γ-secretase modulators. *Eur. J. Pharmacol.* **2017**, *812*, 104−112.
(51) Langosch, D.; Scharnagl, C.; Steiner, H.; Lemberg, M. K. Understanding intramembrane proteolysis: From protein dynamics to reaction kinetics. *Trends Biochem. Sci.* **2015**, *40*, 318−327.
(52) Chávez-Gutiérrez, L.; Bammens, L.; Benilova, I.; Vandersteen, A.; Benurwar, M.; Borgers, M.; Lismont, S.; Zhou, L.; Van Cleynenbreugel, S.; Esselmann, H.; et al. The mechanism of γ-Secretase dysfunction in familial Alzheimer disease. *EMBO J.* **2012**, *31*, 2261−2274.
(53) Takeo, K.; Tanimura, S.; Shinoda, T.; Osawa, S.; Zahariev, I. K.; Takegami, N.; Ishizuka-Katsura, Y.; Shinya, N.; Takagi-Niidome, S.; Tominaga, A.; et al. Allosteric regulation of -secretase activity by a phenylimidazole-type -secretase modulator. *Proc. Natl. Acad. Sci. U.S.A.* **2014**, *111*, 10544−10549.
(54) Somavarapu, A. K.; Kepp, K. P. Loss of stability and hydrophobicity of presenilin 1 mutations causing Alzheimer's disease. *J. Neurochem.* **2016**, *137*, 101−111.
(55) Somavarapu, A. K.; Kepp, K. P. Direct Correlation of Cell Toxicity to Conformational Ensembles of Genetic Aβ Variants. *ACS Chem. Neurosci.* **2015**, *6*, 1990−1996.
(56) Rynearson, K. D.; Buckle, R. N.; Barnes, K. D.; Herr, R. J.; Mayhew, N. J.; Paquette, W. D.; Sakwa, S. A.; Nguyen, P. D.; Johnson, G.; Tanzi, R. E.; et al. Design and synthesis of aminothiazole modulators of the gamma-secretase enzyme. *Bioorg. Med. Chem. Lett.* **2016**, *26*, 3928−3937.
(57) Zhao, Z.; Pissarnitski, D. A.; Huang, X.; Palani, A.; Zhu, Z.; Greenlee, W. J.; Hyde, L. A.; Song, L.; Terracina, G.; Zhang, L.; et al. Discovery of a Tetrahydrobenzisoxazole Series of γ-Secretase Modulators. *ACS Med. Chem. Lett.* **2017**, *8*, 1002−1006.
(58) Wagner, S. L.; Rynearson, K. D.; Duddy, S. K.; Zhang, C.; Nguyen, P. D.; Becker, A.; Vo, U.; Masliah, D.; Monte, L.; Klee, J. B.; et al. Pharmacological and Toxicological Properties of the Potent Oral γ -Secretase Modulator BPN-15606. *J. Pharmacol. Exp. Ther.* **2017**, *362*, 31−44.
(59) Sekioka, R.; Honjo, E.; Honda, S.; Fuji, H.; Akashiba, H.; Mitani, Y.; Yamasaki, S. Discovery of novel scaffolds for γ-secretase modulators without an arylimidazole moiety. *Bioorg. Med. Chem.* **2018**, *26*, 435−442.
(60) Rynearson, K. D.; Tanzi, R. E.; Wagner, S. L. Discovery of potent gamma secretase modulators for the treatment of Alzheimer's disease. *Translational Neuroscience: Fundamental Approaches for Neurological Disorders*; Springer US: Boston, MA, 2016; pp 359−368.
(61) Kim, S.; Thiessen, P. A.; Bolton, E. E.; Chen, J.; Fu, G.; Gindulyte, A.; Han, L.; He, J.; He, S.; Shoemaker, B. A.; et al. PubChem substance and compound databases. *Nucleic Acids Res.* **2015**, *44*, D1202−D1213.
(62) Harder, E.; Damm, W.; Maple, J.; Wu, C.; Reboul, M.; Xiang, J. Y.; Wang, L.; Lupyan, D.; Dahlgren, M. K.; Knight, J. L.; et al. OPLS3: A force field providing broad coverage of drug-like small molecules and proteins. *J. Chem. Theory Comput.* **2015**, *12*, 281−296.
(63) Sierka, M.; Hogekamp, A.; Ahlrichs, R. Fast evaluation of the coulomb potential for electron densities using multipole accelerated resolution of identity approximation. *J. Chem. Phys.* **2003**, *118*, 9136−9148.
(64) Klamt, A.; Schüürmann, G. COSMO: a new approach to dielectric screening in solvents with explicit expressions for the screening energy and its gradient. *J. Chem. Soc. Perkin Trans. 2* **1993**, *5*, 799−805.
(65) Tang, N.; Skibsted, L. H. Zinc bioavailability from phytate-rich foods and zinc supplements. Modeling the effects of food components with oxygen, nitrogen, and sulfur donor ligands. *J. Agric. Food Chem.* **2017**, *65*, 8727−8743.
(66) Trott, O.; Olson, A. J. Autodock Vina: Improving the speed and accuracy of docking with a new scoring function, efficient optimization, and multithreading. *J. Comput. Chem.* **2010**, *31*, 455−461.
(67) Schymkowitz, J.; Borg, J.; Stricher, F.; Nys, R.; Rousseau, F.; Serrano, L. The FoldX web server: An online force field. *Nucleic Acids Res.* **2005**, *33*, W382−W388.
(68) O'Boyle, N. M.; Banck, M.; James, C. A.; Morley, C.; Vandermeersch, T.; Hutchison, G. R. Open Babel: An open chemical toolbox. *J. Cheminf.* **2011**, *3*, 33.
(69) Halgren, T. A.; Murphy, R. B.; Friesner, R. A.; Beard, H. S.; Frye, L. L.; Pollard, W. T.; Banks, J. L. Glide: A New approach for rapid, accurate docking and scoring. 2. enrichment factors in database screening. *J. Med. Chem.* **2004**, *47*, 1750−1759.
(70) Jacobson, M. P.; Pincus, D. L.; Rapp, C. S.; Day, T. J. F.; Honig, B.; Shaw, D. E.; Friesner, R. A. A Hierarchical approach to all-atom protein loop prediction. *Proteins Struct. Funct. Genet.* **2004**, *55*, 351−367.

DOI: 10.1021/acsomega.8b02196
ACS Omega 2018, 3, 18078−18088